Nonlinear Model Predictive Controller for Compensations of Single Line-to-ground Fault in Resonant Grounded Power Distribution Networks

Warnakulasuriya Sonal Prashenajith Fernando, *Student Member*, *IEEE*, Mostafa Barzegar-Kalashani, *Student Member*, *IEEE*, Md Apel Mahmud, *Senior Member*, *IEEE*, Shama Naz Islam, *Member*, *IEEE*, and Nasser Hosseinzadeh

***Abstract*—An nonlinear model predictive controller (NMPC) is proposed in this paper for compensations of single line-to-ground (SLG) faults in resonant grounded power distribution networks (RGPDNs), which reduces the likelihood of power line bushfire due to electric faults. Residual current compensation (RCC) inverters with arc suppression coils (ASCs) in RGPDNs are controlled using the proposed NMPC to provide appropriate compensations during SLG faults. The proposed NMPC is incorporated with the estimation of ASC inductance, where the estimation is carried out based on voltage and current measurements from the neutral point of the distribution network. The compensation scheme is developed in the discrete time using the equivalent circuit of RGPDNs. The proposed NMPC for RCC inverters ensures that the desired current is injected into the neutral point during SLG faults, which is verified through both simulations and control hardware-in-the-loop (CHIL) validations. Comparative results are also presented against an integral sliding mode controller (ISMC) by demonstrating the capability of power line bushfire mitigation.**

***Index Terms*—Fault current, faulty phase voltage, nonlinear model predictive controller (NMPC), parameter adaptation, parametric uncertainty, power line bushfire.**

I. Introduction

FIRE risks in distribution networks are becoming a crucial challenge to system operators due to increases in power line bushfires around the world, especially in Australia and the USA [1]. The risk of power line bushfire can inherently be raised during the summer season when overhead distribution networks touch trees in forests or vegetation as the fault current becomes too high [2]. The resonant grounding technique, commonly referred as the ground fault neutralizer (GFN) or rapid earth fault current limiter (REFCL), is considered as a potential solution for reducing the fault current, which is first adopted by the bushfire prone areas in Victoria, Australian [3]. The REFCL detects single line-to-ground (SLG) faults in the distribution networks and reduces the fault current to a lower value [4]. The REFCL generally operates based on the current-voltage regulation principle, through which a current is injected into the neutral point and the neutral voltage is adjusted to the negative of the faulty phase voltage, mainly for compensating the fault current [5], [6]. However, the adaptation of this new technology introduces several problems such as the network balancing [7] and the appropriate current injected into the neutral point through the residual current compensation (RCC) inverter to fully compensate the fault current [8].

The switching signals of the RCC inverter are regulated by the control schemes similar to traditional inverter controllers. Two preliminary methods based on switched parallel arc suppression coils (ASCs) or switched parallel resistors are presented in [9] and [10] to suppress the overvoltage under the SLG faults in medium-voltage distribution networks. Another switch-based method by adapting an isolation and a zigzag grounding transformer is presented in [11] to limit the ground fault current while constraining the zero-sequence voltage to be opposite to the faulty phase voltage. However, the switching of different elements requires to follow a pre-defined step, which cannot compensate the fault current to the desired level. Another current injection principle is used in [12] for controlling the RCC inverter, which requires to calculate the voltage drop and load current. However, these calculations require some assumptions, which in turn affect the fault current compensation. The proportional-integral (PI) controller in [13] is applied to an inverter topology with both single- and three-phase configurations, where the latter achieves better compensations but it needs three coils. Another PI controller in [14] uses a deterministic approach to calculate the reference current based on leakage resistance and capacitance. References [13] and [14] use traditional modulation technique for the PI controllers and [15] applies an advanced one, but it partially compensates the ca-

Manuscript received: February 10, 2023; revised: August 23, 2023; accepted: February 20, 2024. Date of CrossCheck: February 20, 2024. Date of online publication: April 18, 2024.

W. S. P. Fernando and M. A. Mahmud (corresponding author) are with the Faculty of Engineering and Environment, Northumbria University, Newcastle, UK (e-mail: sonal.fernando@northumbria.ac.uk; md.a.mahmud@northumbria.ac.uk).

M. Barzegar-Kalashani is with the School of Software and Electrical Engineering, Swinburne University of Technology, Hawthorn, Australia (e-mail: mbarzegarkalashani@swin.edu.au).

S. N. Islam and N. Hosseinzadeh are with the School of Engineering, Deakin University, Waurn Ponds, Australia (e-mail: shama.i@deakin.edu.au; nasser.hosseinzadeh@deakin.edu.au)

DOI: 10.35833/MPCE.2023.000065

pacitive fault current. All these PI controllers track a reference with sinusoidal characteristics, which introduce steady-state errors due to the presence of very high harmonic components. The tracking problem related to the fault current compensation is addressed in [16] using the combination of PI and proportional-resonant (PR) controllers, i. e., PI+PR controllers, but the single-loop structure of which could not ensure the desired level of fault compensations.

Controllers with dual-loop structures overcome the limitations of single-loop controllers [17]-[20]. In these dual-loop controllers, the inner loop compensates the fault current while the outer loop generates the reference fault current for the compensation by regulating the voltage. These dual-loop controllers use a similar or different controllers in two loops, e.g., ① PI controllers in both loops [17]; ② PI+PR controller for generating the reference fault current in the outer loop and PI controller for compensating the fault current in the inner loop [18]; ③ magnetically controlled reactor in one loop and active power compensator in the other loop [19]; and ④ and lag compensator in the outer loop and PI controller in the inner loop [20]. Though these controllers are useful for compensating the fault current, their effectiveness is mostly verified under low-impedance faults, while most issues due to the inability to achieve the desired level of faulty phase voltage compensation are under the high-impedance faults. Furthermore, these controllers do not use the physical modeling approach for resonant grounded power distribution networks (RGPDNs).

The linearized models of RGPDNs are used in [21] and [22] to design controllers for RCC inverters. The H-infinity controller in [21] ensures the robust compensation and its implementation is problematic as the order of the controller is very high (the 7^{th} order) even after the order has already been reduced. The two-level linear model predictive controller in [22] requires low sampling frequency and its steady-state performance is better than other controllers. However, this linear controller operates only in some limited situations (mostly under low-impedance faults), and it cannot provide robustness against variations in parameters of the RGPDN. A disturbance rejection controller is proposed in [23] for REFCLs and it can reject the disturbances (mainly external disturbances and parameter variations), which need to be estimated based on extensive frequency-domain analysis. The problems of operating regions and parameter variations are overcome in [24] and [25] by using nonlinear backstepping controller (BSC), where the parametric uncertainty of the adjustable inductor in the GFN is bounded and estimated. However, the BSC in [24] is developed for three-phase ASC while one coil is sufficient for compensating the SLG faults. Though the approach in [25] is developed for single-phase ASC, a phase-locked loop with second-order generalized integrator (SOGI-PLL) is required to calculate the reference fault current, which complicates the control structure. Furthermore, the BSCs considering the bounded parametric uncertainty will only ensure the robustness within a pre-defined bound. Moreover, none of these controllers consider the compensations of faulty phase voltage and fault current to their desired levels for power line bushfire mitigation as given in [3].

A recently designed nonlinear BSC (NBSC) in [26] compensates the fault current and faulty phase voltage by fulfilling the standards for power line bushfire mitigation. This controller is further augmented by adding an additional integrator to the control input [27], which makes an integral BSC (IBSC) with the aim of eliminating the steady-state tracking error seen in [26]. However, both controllers in [26] and [27] require exact parameters of the RGPDN to ensure the desired level of fault compensation. An integral sliding mode controller (ISMC) is presented in [28] and it is capable to ensure the robustness against parametric uncertainties and external disturbances, where an integral sliding surface (SS) is used to avoid the chattering. Another adaptive sliding mode controller (SMC) is used in [29] to combine the benefits of the parameter adaptation scheme and the application of a conventional SS. However, the convergence speed seems to be a problem in [28] and [29], which is overcome in [30] and [31] by introducing advanced SSs with fast reaching laws. A more recent control scheme in [32] combines the PI action to eliminate chattering and a nonsingular fast terminal (NFT) SS to eradicate the singularity problem to form a hybrid controller called PI-NFT-SMC. This hybrid controller takes advantage of both the integral action and the nonsingular SS. Another recent study utilizes a global terminal SS (GT-SS) with a quick reaching law to ensure the rapid convergence of tracking error [33]. All the SMCs discussed above are designed in the continuous time although they are implemented in the discrete time in practice. To improve the feasibility of SMCs in the practical implementation, a discrete SMC (DSMC) is designed in [34], which initially converts the REFCL model to the equivalent *dq* frame and then completes discretization. Though the control schemes in [28]-[34] ensure the desired level of fault compensations following the guidelines of power line bushfire mitigation in RGPDSs under both low- and high-impedance faults, their performances highly rely on the selection of SSs and the control parameters are not optimal. Hence, it is essential to design a controller for the RCC inverter that does not require the selection of such SSs, and the optimal control parameters can inherently be obtained during the design process. The nonlinear model predictive controller (NMPC) proposed in [35] solves the problem of selecting the SS while ensuring the better performance. Similar approaches are also presented in [36]-[38] for other applications. However, all these approaches require the parametric information of REFCL.

Based on the facts arising from existing literature on the control of RCC inverters in the RGPDN, the key limitations of these methods can be summarised as follows.

1) The model-free and model-based linear controllers cannot compensate SLG faults in RGPDNs to a level that can mitigate power line bushfires.

2) The model-free and model-based linear controllers do not consider high-impedance faults.

3) The nonlinear controllers significantly reduce the fault current to a safe level though they require complicated SS and exact parameters for BSCs.

This paper proposes an NMPC for the RCC inverter in an RGPDN to compensate the faulty phase voltage and fault

current under the SLG faults. Here, the value of the adjustable inductor is estimated using the voltage and current measurements from the neutral point of the distribution network. The optimization problem for the proposed NMPC is formulated by incorporating this estimated parameter, which is then solved to achieve the optimal control performance, i.e., the desired level of fault compensation. Therefore, the proposed NMPC will overcome the limitations (especially the bounded uncertainty and non-optimality) of existing nonlinear SMCs. Another important feature of the proposed NMPC is that it determines the optimal control parameters without increasing undesired components in the control signal. The key novel aspects of the proposed NMPC against the previously developed controller in [35] can be summarized as follows.

1) The value of the adjustable inductor is estimated using the actual voltage and current measurements from the neutral point of the distribution network. In contrast, the existing control techniques utilize the nominal value of the adjustable inductor, which can adversely impact the control performance in practice bacause the value of an adjustable inductor can change due to environmental factors, which would require constant re-tuning of the inductor.

2) The values of leakage parameters (such as the resistance and capacitance) also change during the operation, and it is necessary to constantly monitor these changes, which is an arduous task due to the large size of the distribution network. Similarly, this would require constant re-tuning of the adjustable inductor to achieve the resonance condition.

3) The optimization problem for the proposed NMPC is solved based on the estimated inductor, which ensures higher accuracy and faster convergence of the controlled variable, i.e., the injected current into the neutral point in this case, to its reference value.

The performance of the proposed NMPC is evaluated through both simulation and control hardware-in-the-loop (CHIL) platforms under both low- and high-impedence faults in an RGPDN. The results are benchmarked against the performance criteria in [3] for power line bushfire mitigation through ensuring the levels of fault compensation. The superiority of the proposed NMPC are further verified compared with an ISMC in [28].

II. Dynamic Modeling of RCC Inverters in RGPDNs

Figure 1 shows a T-type RCC inverter embedded with the GFN having an adjustable inductor L_p, which is connected to the neutral point of a distribution substation. When the distribution network is considered as a balanced one, the three-phase zero-sequence capacitors and resistances are equal, i.e., $C_{0A}=C_{0B}=C_{0C}=C_0$ and $R_{0A}=R_{0B}=R_{0C}=R_0$, where the subscripts A, B, and C represent the three phases. Under an SLG fault, the inductor L_p is adjusted to resonant with the total zero-sequence capacitor, i.e., $3C_0$. However, the RGPDN actually experiences imbalances in the practical operation, and the network balancing techniques as presented in [7] is used to ensure the balance up to a certain limit (e.g., a maximum residual current of 100 mA). The regulatory impact statement in [3] clearly states the REFCL is only effective if the network is balanced up to this certain limit and it does not work for unbalanced networks. This statement has been made based on a series of experiments that were carried out under different operating conditions. It is important to note that the fault compensation using an ASC will affect the effectiveness of the existing fault detection mechanism because the fault current becomes significantly low and traditional relays are not capable to sense faults. However, the REFCL, which is basically the ASC with an RCC inverter, comes up with its own fault detection mechanism when it starts working. This capability assists to check whether the fault is temporary or permanent. If the fault is temporary, the ASC is activated to mitigate the power line bushfire and then the system continues to operate without the ASC. If the fault is permanent, the feeder is tripped so that power line bushfires are avoided. Figure 1 includes an RCC inverter with an external DC voltage source V_{dc} to inject current i_N to the neutral point. Taking the SLG fault on phase A as an example, the faulty phase voltage v_f becomes the voltage of phase A v_A, i.e., $v_f=v_A$. As shown in Fig. 1, the fault current i_f flowing through the fault impedance R_f can be expressed as:

$$i_f = \frac{v_f}{R_f} = \frac{v_A}{R_f} \tag{1}$$

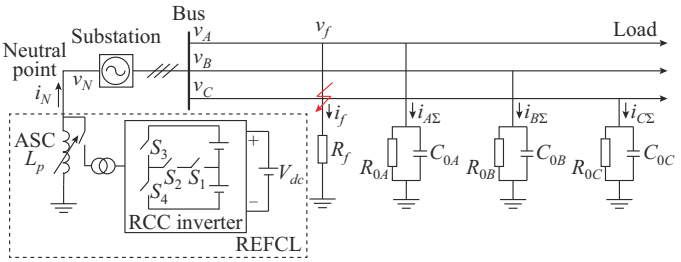

Fig. 1. A test RGPDN for dynamic modeling of REFCL.

Only the reactive component of the fault current i_f can be compensated through L_p. And when $L_p=3C_0$, there is a perfect resonance, which means the reactive component of i_f will be fully compensated. However, in practice, there also exists a significant active component of i_f, which can be enough to keep the resultant fault characteristics and cause bushfires. The RCC inverter driven by a set of switching signals (S_1-S_4) regulates the injected current into the neutral point i_N to compensate i_f and assists to keep the faulty phase voltage to a safe level. The expression of i_N under an SLG fault can be expressed as:

$$i_N = i_f + i_{A\Sigma} + i_{B\Sigma} + i_{C\Sigma} \tag{2}$$

where $i_{X\Sigma}$ ($X=\{A,B,C\}$) is the total current flowing through shunt branch on phase X, which can be expressed as:

$$i_{X\Sigma} = \frac{v_X}{R_0} + C_0\frac{\mathrm{d}v_X}{\mathrm{d}t} \tag{3}$$

where v_X is the phase voltage.

Hence, by substituting (3) into (2), we can obtain:

$$i_N = \frac{v_A}{R_f} + \frac{v_A+v_B+v_C}{R_0} + C_0\frac{\mathrm{d}}{\mathrm{d}t}(v_A+v_B+v_C) \tag{4}$$

As shown in Fig. 1, the REFCL is installed on the neutral point of a distribution substation to inject current for neutral-

izing SLG faults. Therefore, the dynamic model of the injected current i_N should include the properties of the substation. Hence, the effect of the line reactance will be incorporated into i_N for the fault current compensation. It is also worth to note that there might be so many external feeders in a substation with lots of branches. The effects of all these external feeders including their transient behaviors can be incorporated into i_N, because any changes on any parts of the network will affect the value of i_N at the substation.

The phase-to-neutral voltage e_{XN} represents the difference between the phase voltage v_X and the neutral voltage v_N, i.e.,

$$e_{XN}=v_X-v_N \tag{5}$$

Equation (5) can be expanded as:

$$\begin{cases} v_A=e_{AN}+v_N \\ v_B=e_{BN}+v_N \\ v_C=e_{CN}+v_N \end{cases} \tag{6}$$

It is well-known that $e_{AN}+e_{BN}+e_{CN}=0$ for a balanced system, based on which the sum of all phase voltages can be written as:

$$v_A+v_B+v_C=3v_N \tag{7}$$

Hence, (4) can be simplified as:

$$i_N=\frac{v_A}{R_f}+3\frac{v_N}{R_0}+3C_0\frac{\mathrm{d}v_N}{\mathrm{d}t} \tag{8}$$

At this stage, it is required to find the reference value of i_N, which is denoted as i_N^{ref}. Taking the SLG fault on phase A as an example, v_N can be expressed in terms of the faulty phase voltage according to (5), i.e., $v_N=v_A-e_{AN}$. Hence, (8) can be written as:

$$i_N=\left(\frac{3v_A}{R_0}+\frac{v_A}{R_f}\right)+3C_0\frac{\mathrm{d}v_A}{\mathrm{d}t}-3\left(\frac{e_{AN}}{R_0}+C_0\frac{\mathrm{d}e_{AN}}{\mathrm{d}t}\right) \tag{9}$$

The last term on the right side of (9) corresponds to the effect of the SLG fault on phase A [25]. Hence, the value of i_N^{ref}, fully eliminating the fault current, i.e., making $i_f=0$, can be derived from (9) as:

$$i_N^{ref}=-\left(\frac{3}{R_0}e_{AN}+3C_0\frac{\mathrm{d}e_{AN}}{\mathrm{d}t}\right) \tag{10}$$

Please note that e_{AN}, which is an instantaneous signal, has the sinusoidal behavior, and thus $\mathrm{d}e_{AN}/\mathrm{d}t\neq 0$. It can be observed from (10) that the value of i_N^{ref} does not depend on the fault impedance. If i_N is set to be i_N^{ref} through the control action, the faulty phase voltage $v_A=v_f$ can be quickly controlled to be zero, and thus setting the fault current i_f to be zero as per in (1). The injected current into the neutral point by the RCC inverter needs to be controlled by controlling the changes in i_N, i.e., $\mathrm{d}i_N/\mathrm{d}t$, which can be obtained by applying Kirchhoff's laws to the neutral point of the distribution network shown in Fig. 1. Therefore, it is possible to obtain the voltage drop across L_p as: $L_p\mathrm{d}i_N/\mathrm{d}t+v_N=mV_{dc}$, where mV_{dc} is the output voltage of the RCC inverter [39], and m is the modulation index. This equation can be re-arranged to obtain $\mathrm{d}i_N/\mathrm{d}t$ as:

$$\frac{\mathrm{d}i_N}{\mathrm{d}t}=\frac{mV_{dc}-v_N}{L_p} \tag{11}$$

In this paper, the modulation index m is the modulating signal or control input for the RCC inverter, which is designed using an NMPC.

III. Equivalent Discrete-time Modeling of RCC Inverters in RGPDNs

For an RCC inverter, its modulation index m is its output voltage divided by its input voltage. For a single switching instant in an RCC inverter, the input voltage is $V_{dc}/2$. Considering the output voltage as $v(t)$ (or simply v), m can be represented as [39]:

$$m=\frac{2v}{V_{dc}} \tag{12}$$

Taking v as the controlled variable for i_N, the value of $\mathrm{d}i_N/\mathrm{d}t$ can be rewritten as (13) by substituting (12) into (11).

$$\frac{\mathrm{d}i_N}{\mathrm{d}t}=\frac{2}{L_p}v-\frac{1}{L_p}v_N \tag{13}$$

By replacing i_N with x and v_N with ζ, (13) can be generalized as:

$$\dot{x}=\frac{2}{L_p}v-\frac{1}{L_p}\zeta \tag{14}$$

Equation (14) can be solved with any initial values and its solution can be written as:

$$x(t)=\phi(t_0,x_0,v,\zeta):=x_0+\int_0^t\left(\frac{2}{L_p}v(\tau)-\frac{1}{L_p}\zeta(\tau)\right)\mathrm{d}\tau \tag{15}$$

where the subscript 0 means the initial value.

The discrete-time system can be obtained by considering the sampling instant as k ($k=0,1,\ldots,N$), where N is the horizon, and the sampling period $T>0$ can be obtained with a regular sampling time $t_n=kT$. In order to make a distinction between the continuous- and discrete-time systems, v in the continuous-time system is represented by u in the discrete-time system. For this reason, u is the original control signal to drive the RCC inverter. Therefore, the equivalent discrete-time model of the RCC inverter in an RGPDN can be written as:

$$x_{k+1}=f(x_k,u_k,\zeta_k):=\phi(T,0,x_k,u_k,\zeta_k)=x_k+\int_0^T\left(\frac{2}{L_P}u(\tau)-\frac{1}{L_P}\zeta(\tau)\right)\mathrm{d}\tau \tag{16}$$

If u and ζ are constants over a period of T, (16) can be simplified as [40]:

$$x_{k+1}=x_k+\frac{2T}{L_p}u_k-\frac{T}{L_p}\zeta_k \tag{17}$$

From (17), it is clear that the dynamic injected current depends on the inductor L_p. Therefore, by obtaining the value of L_p from the measurements of v_N and i_N, the proper control of the injected current can be ensured.

IV. Design of Proposed NMPC and a Brief Overview of ISMC

A. Estimation of L_p

Initially, the parameter L_p is completely unknown. Letting $\theta=1/L_p$, the discrete-time model in (17) can be written as:

$$x_{k+1}=x_k+T(2u_k-\zeta_k)\theta \tag{18}$$

From Fig. 1, it is clear that the voltage across the inductor L_p can be calculated as:

$$v_N = sL_p i_N \tag{19}$$

where $s = j\omega$ is the complex operator, and ω is the angular frequency. Denote $\hat{\theta}$ as the estimated value of θ, which can be derived from (19) as:

$$\hat{\theta} = \left| \frac{si_N}{v_N} \right| \tag{20}$$

This estimated value of θ is used for the proposed NMPC rather than its nominal value.

B. Design of Proposed NMPC

As indicated earlier, the design of the proposed NMPC involves the formulation of the optimization problem and the solution of this problem. A cost function ℓ is defined initially for a particular prediction horizon N, and this cost function should include the information related to the state (x), control input (u), and estimated value of the unknown parameter ($\hat{\theta}$). The main control objective is to make sure that the injected current accurately tracks its reference and therefore, the cost function is designed to penalize the error between the state x and its reference x^{ref}. With all these considerations, the associated objective or cost function can be defined as:

$$\ell(n, x_k, u_k, \hat{\theta}) = (x_k - x_k^{ref})^2 + \lambda u_k^2 + \hat{\theta}_k^2 \tag{21}$$

where x_k^{ref} corresponds to the reference current i_N^{ref}; n denotes the instant of the current state; and $\lambda \geq 0$ is a weighting parameter considering the influence of the control input u on the cost function ℓ, which makes sure that the control input u is effective in zeroing the error between x_k and x_k^{ref}.

The performance index J_N for a prediction horizon of N can be computed as [40]:

$$\begin{cases} J_N(n, x, u(\cdot), \hat{\theta}, \zeta) := \sum_{k=0}^{N-1} \ell(n+k, x_{u,k}, u_k, \hat{\theta}_k) \\ \text{s.t.} \quad x_{u,0} = x_0 \\ \qquad x_{u,k+1} = x_k + T(2u_k - \zeta_k)\hat{\theta}_k \end{cases} \tag{22}$$

where $x_{u,k}$ gives the predicted trajectory of the state x_k.

Equation (22) is an optimization problem that can be minimized to make sure that the cost function ℓ is zero. Therefore, by solving this optimization problem, it is possible to obtain an optimal solution u_k that can make the cost function be zero. When $N = 2$, (22) can be written as:

$$J_2 = \sum_{k=0}^{1} \ell(n+k, x_{u,k}, u_k, \hat{\theta}_k) \tag{23}$$

$$J_2 = \ell(n+0, x_{u,0}, u_0, \hat{\theta}_0) + \ell(n+1, x_{u,1}, u_1, \hat{\theta}_1) \tag{24}$$

where $J_2 = J_2(n, x, u(\cdot), \hat{\theta}, \zeta)$.

Using the value of ℓ obtained from (21), (24) can be rewritten as:

$$J_2 = (x_{u,0} - x_{n+0}^{ref})^2 + \lambda u_0^2 + \hat{\theta}_0^2 + (x_{u,1} - x_{n+1}^{ref})^2 + \lambda u_1^2 + \hat{\theta}_1^2 \tag{25}$$

Furthermore, from (22), the following equations are valid:

$$\begin{cases} x_{u,0} = x_0 \\ x_{u,1} = x_0 + T(2u_0 - \zeta_0)\hat{\theta}_0 \end{cases} \tag{26}$$

Using (26), (25) can be written as:

$$J_2 = (x_0 - x_{n+0}^{ref})^2 + \lambda u_0^2 + \hat{\theta}_0^2 + [x_0 + T\hat{\theta}_0(2u_0 - \zeta_0) - x_{n+1}^{ref}]^2 + \lambda u_1^2 + \hat{\theta}_1^2 \tag{27}$$

The performance index J_2 in (27) is minimized only with respect to u_0 because u_1 does not have any effects on the trajectories of $x_{u,0}$ and $x_{u,1}$, and the concept of receding horizon (i.e., using the first horizon as the control signal) is used in this paper. Hence, the optimal condition for J_2 can be expressed by equating the partial derivative of J_2 with respect to u_0 to zero, i.e., $\partial J_2 / \partial u_0 = 0$, which can be calculated from (27) as:

$$\frac{\partial J_2}{\partial u_0} = 2\lambda u_0 + 2 \times 2T\hat{\theta}_0[x_0 + T\hat{\theta}_0(2u_0 - \zeta_0) - x_{n+1}^{ref}] = 0 \tag{28}$$

$$u_0[2\lambda + 8(T\hat{\theta}_0)^2] + 4T\hat{\theta}_0(x_0 - T\hat{\theta}_0\zeta_0 - x_{n+1}^{ref}) = 0 \tag{29}$$

From (29), the optimal value of u_0, i.e., u_0^*, can be determined as:

$$u_0^* = \frac{-2T\hat{\theta}_0(x_0 - x_{n+1}^{ref} - T\hat{\theta}_0\zeta_0)}{\lambda + 4(T\hat{\theta}_0)^2} \tag{30}$$

And the optimal control law of the proposed NMPC can be represented as:

$$\mu_2(n, x_k) = \frac{-2T\hat{\theta}_k(x_k - x_{n+1}^{ref} - T\hat{\theta}_k\zeta_k)}{\lambda + 4(T\hat{\theta}_k)^2} \tag{31}$$

where $\mu_2(n, x_k)$ represents the optimal control input when $N = 2$. And then, $\hat{\theta}$ calculated using (20) is fed to (31) to optimally compensate the fault characteristics.

The overall flowchart of the proposed NMPC is shown in Fig. 2, where the model of RCC inverter is discretized and the unknown parameter θ is then defined. The unknown parameter θ is estimated using the voltage and current measurements from the neutral point of the distribution network using (20), which is then utilized for formulating the optimization problem. Finally, this optimization problem is solved to determine the control sequence and the concept of receding horizon is utilized to determine the final control input.

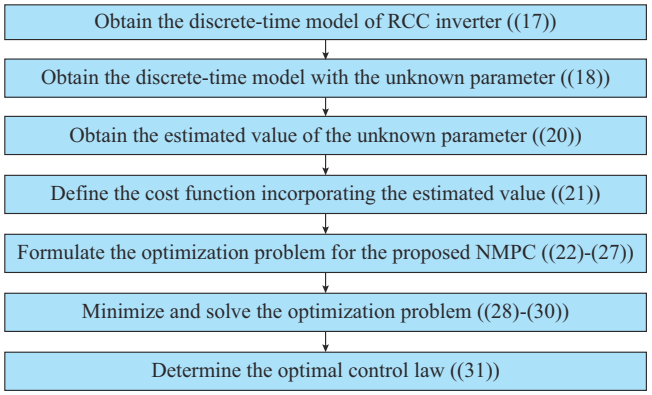

Fig. 2. Overall flowchart of proposed NMPC.

Figure 3 gives the block diagram for the implementation of the proposed NMPC. The outputs are i_N and v_N. The estimated value $\hat{\theta}_k$ is obtained using the measurements of i_N and v_N. Subsequently, the optimal control law of the proposed NMPC given in (31) uses i_N and $\hat{\theta}_k$ to eliminate the error be-

tween the injected current i_N, i.e., x_k, and its reference x_k^{ref} by producing the control signal $\mu_2(n, x_k)$. This control signal is fed to the RCC inverter in the distribution network to ensure that i_N accurately tracks its reference, and then it is possible to completely neutralize the SLG fault.

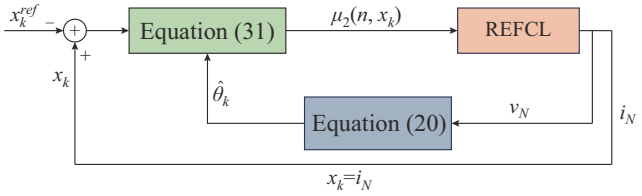

Fig. 3. Block diagram for implementation of proposed NMPC.

The performance analysis of the proposed NMPC is presented in the next section. An ISMC is utilized to compare with the proposed NMPC, and its brief overview is presented in the Supplementary Material.

V. Performance Analysis of Proposed NMPC for RCC Inverters in RGPDNs

In this work, the key control objective of the proposed NMPC is to inject the desired current to the neutral point using the RCC inverter in an RGPDN. Subsequently, this current assures that the faulty phase voltage and fault current are compensated to their desired levels for power line bushfire mitigation as given in [3]. The unknown parameter θ is obtained using (20) via the voltage and current measurements from the neutral point of the distribution network and is incorporated with the optimal control law. During the implementation, only the final parameter estimation in (20) and the optimal control law of the proposed NMPC in (31) are required. The obtained optimal control law ensures accurate tracking of the reference injected current.

The performance of the proposed NMPC is analyzed based on the RGPDN shown in Fig. 1 by applying SLG faults on phase *A*. The scenarios for analyzing the performance include SLG faults under both low and high impedances. The performance analysis is first carried out using MATLAB/Simulink based on the practical network information. The results are further validated by using the real-time simulator OPAL-RT OP5707XG through CHIL validations as there are some safety, confidentiality, and security issues to access the available facilities from the distribution network operator or establish a lab experiment. The performance of the proposed NMPC is benchmarked against the performance criteria in [3] to compensate fault behaviors including a comparative study with the ISMC in [28].

A. Parametric Information of Test RGPDN

The RGPDN is basically a 22 kV (line-to-line) network with an RCC inverter, which is mounted on the neutral point through transformer to step-up the voltage. The values of R_0 and C_0 are taken as 28 kΩ and 4 μF, respectively. It is worth mentioning that these values are selected based on the current industry standard for RGPDN in bushfire prone areas. The RGPDN in Fig. 1 experiences the resonant condition with the ASC when the value of L_p is around 0.9 H, and hence the estimated value of L_p should be around 0.9 H. The load of each phase is 400 Ω and the DC voltage source is rated at 800 V. The modulation scheme to generate switching pulses for the RCC inverter is based on phase opposition disposition approach as discussed in [41], where the switching frequency f_s is 10 kHz.

The control parameter for the proposed NMPC is selected as $\lambda = 3000/f_s^2$ to ensure that both faulty phase voltage and fault current are adequately compensated. This value was found through trial-and-error of the simulations although artificial intelligence (AI) based techniques can be incorporated to fine-tune these values and improve the current and voltage responses obtained from the simulations, which is beyond the scope of this paper. The control parameters ψ and β for the ISMC are selected in a similar way, which are 700 and 500, respectively. The performance of the proposed NMPC is analyzed by considering these control parameters and it is not highly sensitive to the variations in these control parameters easing the tedious parameter selection process.

B. Performance Criteria for Powerline Bushfire Mitigation

Most of the existing literature does not compensate both current and voltage, and even if they are both considered, there are no indications about the timeframe and the magnitudes of current and voltage required to extinguish power line bushfires due to SLG faults on distribution networks in bushfire prone zones. The regulatory impact statement in [3] clearly indicates that the fault current should be limited to a value equal to or less than 0.5 A within 2 s after initiating the compensation using the RCC inverter irrespective of fault impedances, i.e., for both low ($R_f < 1$ kΩ) and high ($R_f \geq 1$ kΩ) impedance faults. At the same time, the faulty phase voltage under low impedances should be monitored at three time instants, i.e., 85 ms, 0.5 s, and 2 s after the activation of the RCC inverter, and it is required to be maintained at or below 1900 V, 750 V, and 250 V, respectively. On the contrary, under high-impedance faults, the faulty phase voltage should be monitored only at 2 s after the activation of the RCC inverte and it is required to be maintained at or below 250 V.

C. Simulation Results

To analyze the performance of the proposed NMPC, the RGPDN is simulated under two SLG faults with $R_f = 120$ Ω and $R_f = 26$ kΩ to cover both low- and high-impedance faults, i.e., a wide range of fault conditions. The performance of the proposed NMPC via both simulation and CHIL validation is analyzed, and the compensation is initiated at the same instant. All the simulation results are assessed against the performance criteria in [3].

The simulation is first conducted under an SLG fault on phase *A* at $t = 0.4$ s with $R_f = 120$ Ω. Figure 4 shows the instantaneous and root mean square (RMS) values of the fault current with the proposed NMPC and ISMC with $R_f = 120$ Ω, where a peak can be found at the instant of an SLG fault. Although it is extremely hard to see the difference in the performance of the proposed NMPC and ISMC from the instantaneous values, it can be easily distinguished from the RMS values. The RMS values show that the ISMC

cannot manage the fault current less than 0.5 A even after the compensation lasts for 2 s while the proposed NMPC brings it down to 0.1588 A, which is below the performance criteria in [3].

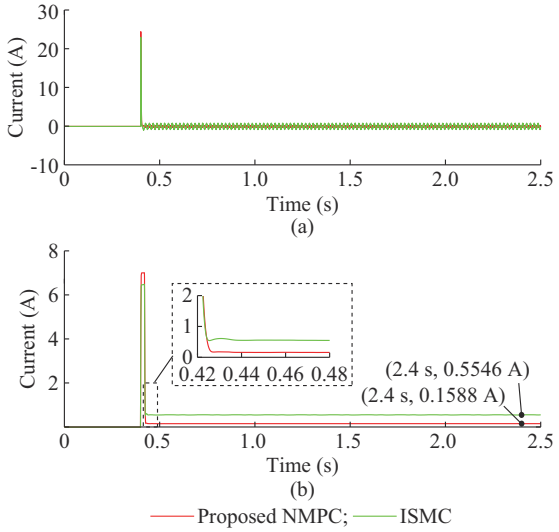

Fig. 4. Instantaneous and RMS values of fault current with proposed NMPC and ISMC with $R_f = 120\ \Omega$. (a) Instantaneous values. (b) RMS values.

Figure 5 shows the instantaneous and RMS values of faulty phase voltage with the proposed NMPC and ISMC with $R_f = 120\ \Omega$. It can be observed that both the proposed NMPC and ISMC can maintain the faulty phase voltage lower than the desired level at all three time instants, i.e., 0.485 s, 0.9 s, and 2.4 s.

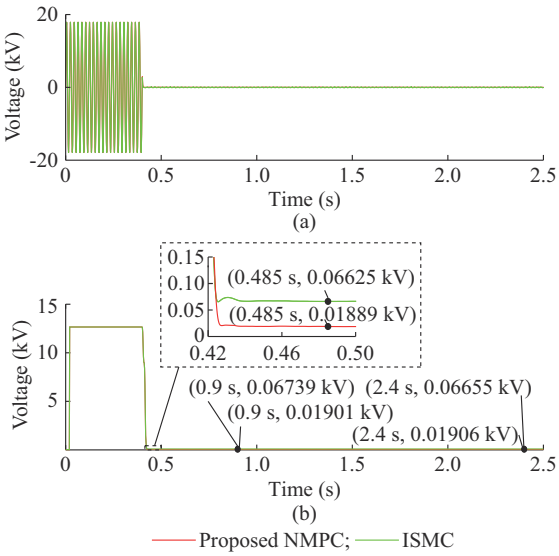

Fig. 5. Instantaneous and RMS values of faulty phase voltage with proposed NMPC and ISMC with $R_f = 120\ \Omega$. (a) Instantaneous values. (b) RMS values.

Table I summarizes the RMS values of the faulty phase voltage at three time instants, demonstrating that the compensated faulty phase voltage using the proposed NMPC reduces to a lower value than that using the ISMC.

TABLE I
RMS VALUES OF FAULTY PHASE VOLTAGE AT THREE TIME INSTANTS

Time instant (s)	RMS value of faulty phase voltage (V)	
	Proposed NMPC	ISMC
0.485	18.89	66.25
0.900	19.01	67.39
2.400	19.06	66.55

The estimated value of L_p with $R_f = 120\ \Omega$ is given in Fig. 6, which is around 0.85 H as can be observed. To achieve the resonance condition for $C_0 = 4\ \mu$F, it is required to tune the inductance value of L_p around 0.85 H, which further confirms the validity of the estimated value of L_p.

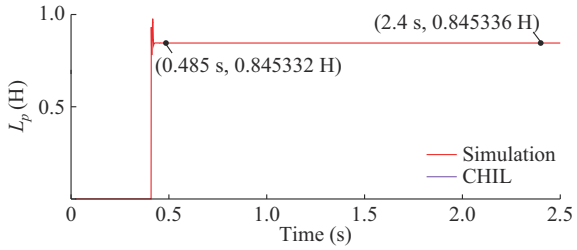

Fig. 6. Estimated value of L_p with $R_f = 120\ \Omega$.

The performance of the proposed NMPC is further analyzed by observing the instantaneous and RMS values of current injected into neutral point with $R_f = 120\ \Omega$, as shown in Fig. 7, with a comparision with ISMC.

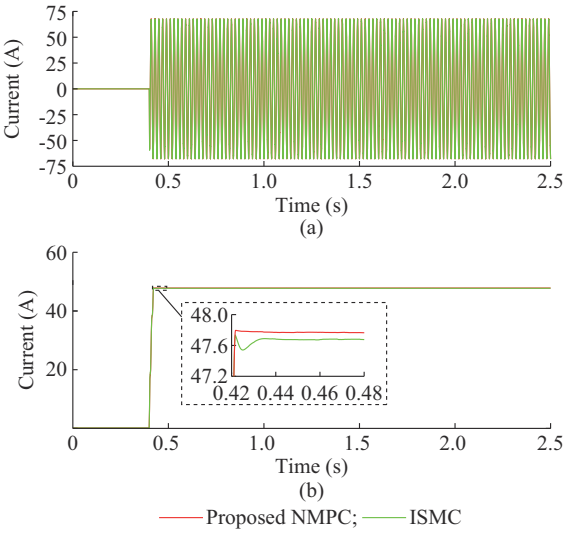

Fig. 7. Instantaneous and RMS values of current injected into neutral point with proposed NMPC and ISMC with $R_f = 120\ \Omega$. (a) Instantaneous values. (b) RMS values.

Both of the proposed NMPC and ISMC ensure the proper reference current tracking though there is a small difference between them. The proper tracking is important for compensating the faulty phase voltage because the current injected into neutral point makes the neutral voltage v_N increase up to a magnitude equal to the faulty phase voltage, i.e., v_A, but in the opposite direction. In this way, the faulty phase voltage needs to reduce to a lower value, which in turn elimi-

nates power line bushfire risks. It is calculated that the value of i_N^{ref} is 47.9 A while the RMS values of i_N with the proposed NMPC and ISMC are 47.76 A and 47.67 A, respectively. Hence, the accuracy of the proposed NMPC is slightly higher than that of the ISMC, which further supports the findings as discussed earlier.

Then, the simulation is conducted under an SLG fault on phase A at $t=0.4$ s with $R_f=26$ kΩ. As can be observed from Fig. 8, the fault current is very low, and the maximum value of the fault current reaches 0.18 A when the SLG fault occurs. After the proposed NMPC and ISMC are applied, the fault currents are both compensated to very low values. Hence, the compensated fault current is well below the limit of 0.5 A.

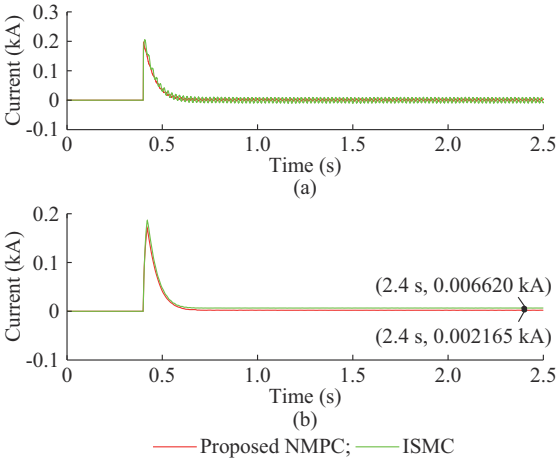

Fig. 8. Instantaneous and RMS values of fault current with proposed NMPC and ISMC with $R_f=26$ kΩ. (a) Instantaneous values. (b) RMS values.

The instantaneous and RMS values of faulty phase voltage in Fig. 9 shows the rapid reduction soon after activating the RCC inverter. As per the performance criteria in [3], this faulty phase voltage is observed at 2.4 s, which is 172 V and 56.3 V when the ISMC and the proposed NMPC are used, respectively. These values are maintained below 250 V, which indicates that both ISMC and the proposed NMPC satisfy the fault compensation criteria for mitigating power line bushfires.

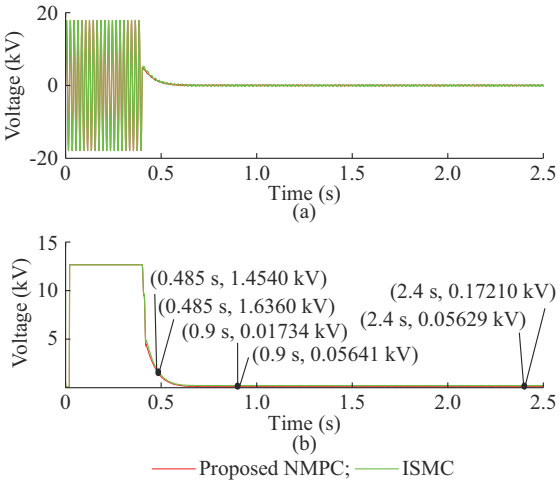

Fig. 9. Instantaneous and RMS values of faulty phase voltage with proposed NMPC and ISMC with $R_f=26$ kΩ. (a) Instantaneous values. (b) RMS values.

The estimated value of L_p with $R_f=26$ kΩ is given in Fig. 10. L_p is tuned to match the capacitance C_0 in the distribution network, which is independent of the fault impedance. Hence, L_p is also estimated as 0.85 H.

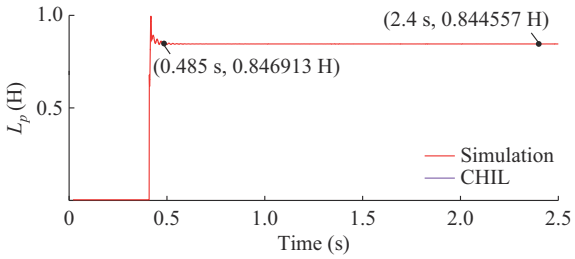

Fig. 10. Estimated value of L_p with $R_f=26$ kΩ.

From the instantaneous and RMS values of the current injected into neutral point in Fig. 11, it can be observed that the injected current is independent of the fault impedance because the control action actually ensures the proper compensation of the faulty phase voltage in a similar way as under low-impedance fault. Therefore, the proposed NMPC compensates the SLG fault in a better way for a wide variation of fault impedances while compared with the ISMC.

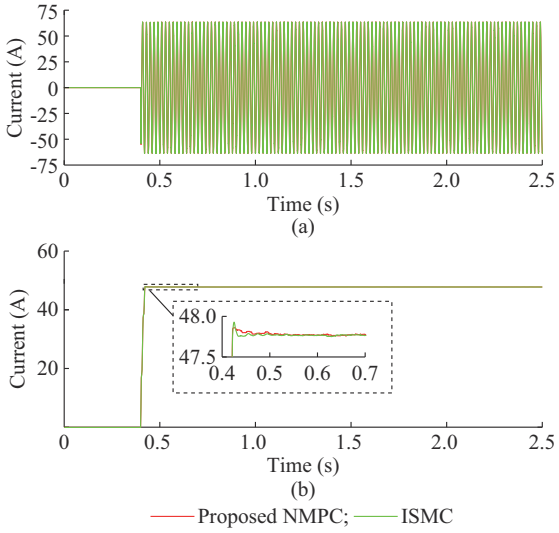

Fig. 11. Instantaneous and RMS values of current injected into neutral point with proposed NMPC and ISMC with $R_f=26$ kΩ. (a) Instantaneous values. (b) RMS values.

Figures 12 and 13 present the instantaneous and RMS values for the output currents of RCC inverter with $R_f=120$ Ω and $R_f=26$ kΩ, respectively. The active and reactive components of these currents with $R_f=120$ Ω and $R_f=26$ kΩ are shown in Figs. 14 and 15, respectively. It can be observed that the output current of RCC inverter mainly consists of the reactive part, because fault current during the SLG fault is mainly capacitive due to the presence of the dominant distributed capacitance. Hence, an equivalent reactive (inductive) current output from the RCC inverter is required to neutralize the capacitive fault current. The residual current, which is the active part, is neutralized by the active component of the current injected by the RCC inverter.

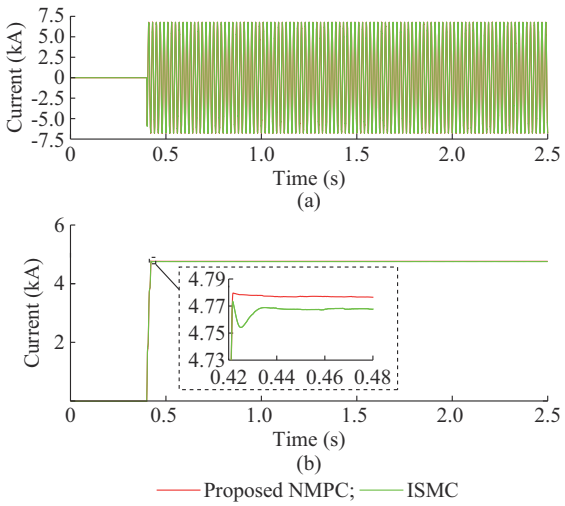

Fig. 12. Instantaneous and RMS values for output current of RCC inverter with $R_f = 120\ \Omega$. (a) Instantaneous values. (b) RMS values.

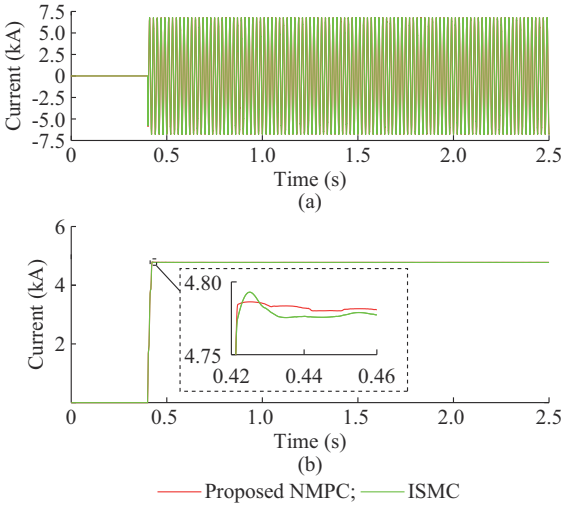

Fig. 13. Instantaneous and RMS values for output current of RCC inverter with $R_f = 26$ kΩ. (a) Instantaneous values. (b) RMS values.

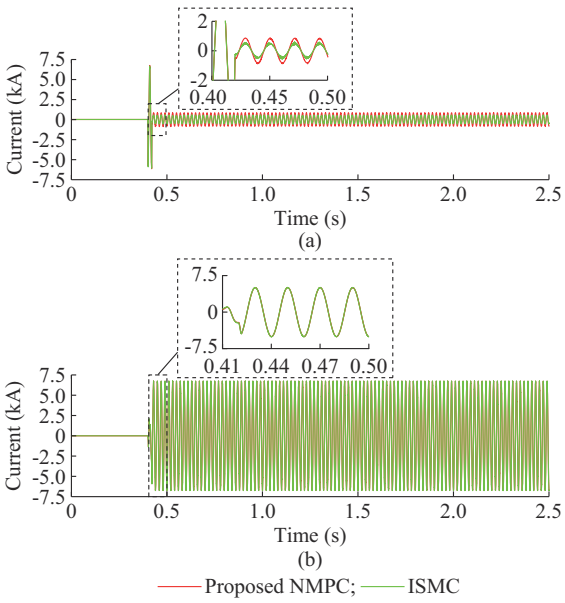

Fig. 14. Active and reactive components of output current of RCC inverter with $R_f = 120\ \Omega$. (a) Active component. (b) Reactive component.

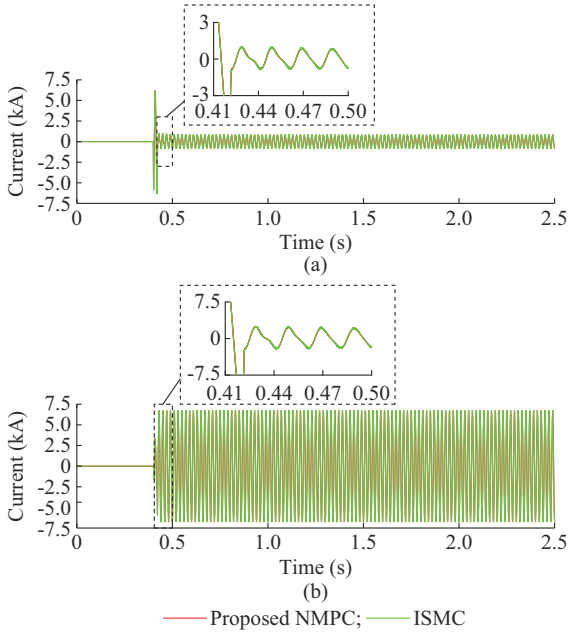

Fig. 15. Active and reactive components of output current of RCC inverter with $R_f = 26$ kΩ. (a) Active component. (b) Reactive component.

Table II gives a comparison of existing control methods for the compensation of SLG faults in RGPDNs. As it can be observed, the compensations for both fault current and faulty phase voltage are considered only in some recently developed nonlinear controllers such as the BSC, SMC, and the proposed NMPC. It is crucial to ensure the compensation of the faulty phase current to prevent electric arcs that might ignite bushfires. At the same time, it is also necessary to compensate the faulty phase voltage; otherwise, this can lead to further complications of double line-to-ground faults or even three-phase faults.

D. CHIL Validation

CHIL validations are carried out with the real-time simulator OPAL-RT OP57075XG to validate the feasibility of the proposed NMPC. CHIL validations has an advantage over the scaled-down experimental setups because the CHIL validations can be performed in real time with the actual distribution network voltages. This provides a clear insight into the performance of the proposed NMPC and how effective it is in meeting the bushfire mitigation guidelines in [3]. The OPAL-RT OP5707XG consists of an Intel Xeon 3.8 GHz CPU and a Xilinx Virtex-7 485T field programming gate array (FPGA). The test distribution network with RCC inverter used in Simulink is deployed onto the FPGA, which has a sampling time of $t_{FPGA} = 215$ ns and runs in real time. The proposed NMPC is deployed on the CPU in the real-time simulator with a sampling time of $t_{CPU} = 5$ μs using the RT-LAB software. In CHIL validations, the distribution network model in the FPGA sends the voltage and current measurements to the proposed NMPC on the CPU and the proposed NMPC processes these signals based on the optimal control law given in (31) and sends a set of switching pulses back to the FPGA to control the RCC inverter. Figure 16 shows the working process of the CHIL validation and Fig. 17 gives the experimental setup with the OPAL-RT simulator.

TABEL II
COMPARISON OF EXISTING CONTROL METHODS FOR COMPENSATION OF SLG FAULTS IN RGPDNS

Control method	Fault impedance (Ω)	Compensated fault current (A)	Compensated faulty phase voltage (V)
Closed-loop	50-2000	0.067-0.026	3.4-50.2
PI	50	7	
PI+advanced topology	2000	7 (single-phase), 1 (three-phase)	
PI+advanced modulation	10-100	4.14-4.67	
PR+PI	Load variation		21
PI+PI	25	0.006	0.16
Lag and PI	10-100	0.16-0.32	
PI+PR and P	100-10000		5-15
Multiple PI and hysteresis	65	0.6	
H-infinity		0.2	
FC-MPC	10-1000	≤3.1	
BSC	1-100	<1.7	
BSC-SOGI-PLL	1-1000	0.0026-0.0600	
NBSC	350-16000	0.0023-0.1286	43-45
IBSC	50-26000	0.003-0.161	23-50
ISMC	100-26000	0.00658-0.56000	56-171
A-SMC	120-25400	0.0025-0.1510	19-44
NT-SMC	250-26000	0.0021-0.4200	50-95
NFT-SMC	400-25400	0.0023-0.0920	37-46
PI-NFT-SMC	300-25400	0.0019-0.1130	33.3-36.4
GT-SMC	80-26000	0.00044-0.01000	10.4-11.54
NMPC	400-26000	0.0016-0.0780	31.36-42.54

Note: BSC-SOGI-PLL is short for BSC with SOGI-PLL; FC-MPC is short for MPC with finite control; and NT-SMC is short for nonsingular terminal SMC.

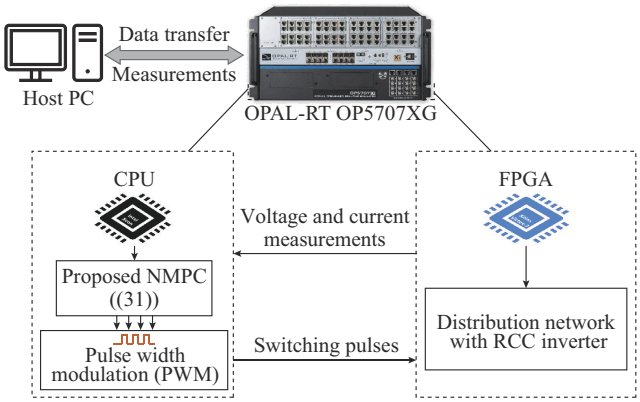

Fig. 16. Working process of CHIL validation.

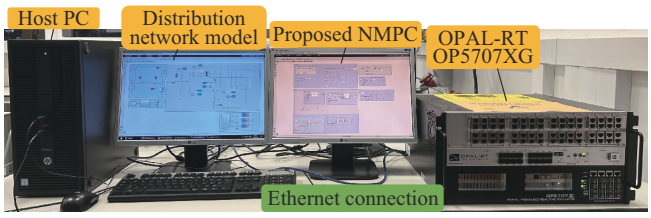

Fig. 17. Experimental setup with OPAL-RT simulator.

CHIL validation results are provided for the proposed NMPC under both the low- and high-impedance faults. Figure 18 gives the instantaneous and RMS values of fault current with $R_f = 120\ \Omega$ for the CHIL validation. For comparison, the simulation result has also been included. As can be observed from Fig. 18, the RMS value of the fault current is well below the limit of 0.5 A for the CHIL validation. There is a slight deviation from the simulation result because the test distribution network runs on the FPGA at a much higher sampling frequency compared with the CPU, where the proposed NMPC is deployed. Therefore, there is a bottleneck of data transfer, which leads to a slight deviation. The test distribution network runs in real time on the FPGA, so it can reflect the performance of the proposed NMPC as if it were implemented onto an actual distribution network.

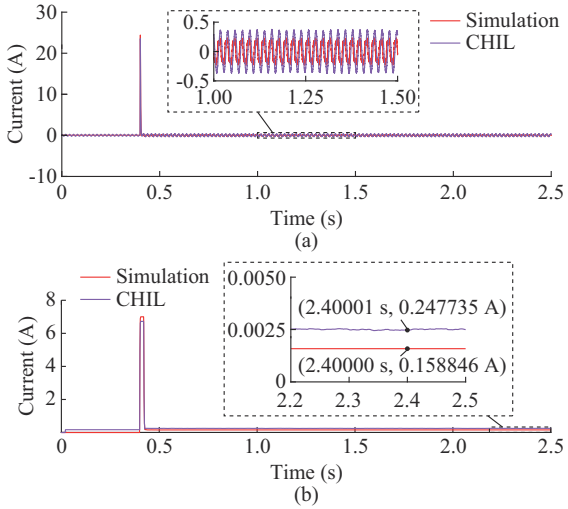

Fig. 18. Instantaneous and RMS values of fault current with $R_f = 120\ \Omega$ for CHIL validation. (a) Instantaneous values. (b) RMS values.

Figure 19 gives the instantaneous and RMS values of faulty phase voltage with $R_f = 120\ \Omega$ for CHIL validation. The RMS value of faulty phase voltage decreases almost instantaneously to about 30 V, which well meets the requirements given in [3]. Similar to the fault current, a slight deviation exists between the simulation and CHIL validation.

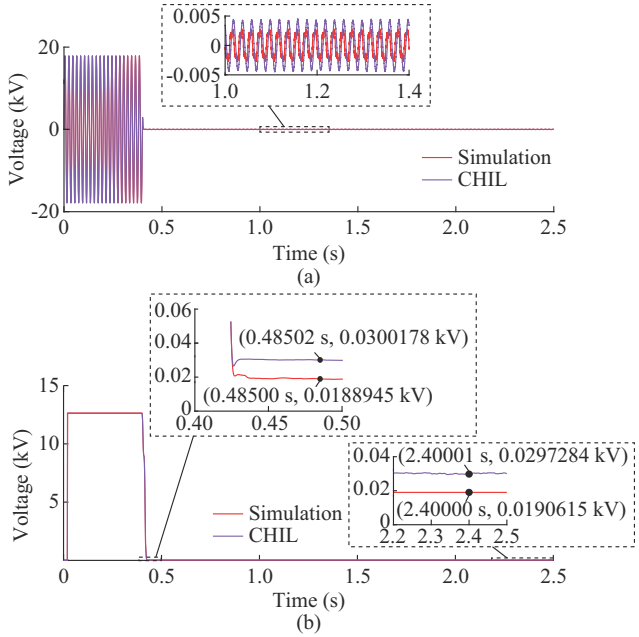

Fig. 19. Instantaneous and RMS values of faulty phase voltage with $R_f = 120\ \Omega$ for CHIL validation. (a) Instantaneous values. (b) RMS values.

Figure 20 gives the estimated value of L_p, using v_N and i_N obtained from the distribution network running on the FPGA, with $R_f = 120\ \Omega$ for CHIL validation. Equation (20) is implemented directly on the OPAL-RT CPU, so there is no bottleneck of data here. Hence, the discrepancy between simulation and CHIL validations is much less.

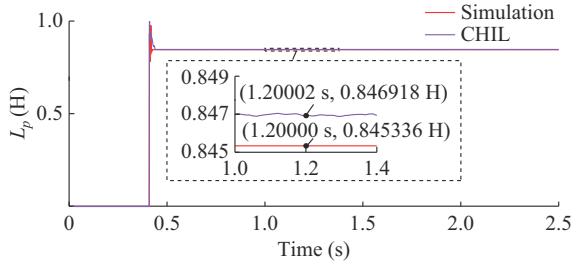

Fig. 20. Estimated value of L_p with $R_f = 120\ \Omega$ for CHIL validation.

Figures 21 and 22 give the instantaneous and RMS values of fault current and faulty phase voltage with $R_f = 26$ kΩ for the CHIL validation. In this high-impedance case, more attention should be given to the compensation of faulty phase voltage. According to the CHIL validation results shown in Fig. 22, the proposed NMPC can adequately compensate the faulty phase voltage. Figure 23 gives the estimated value of L_p with $R_f = 26$ kΩ for the CHIL validation. The CHIL validation results under both the low and high impedances show that the proposed NMPC can be successfully deployed and executed in a real-time environment as the compensated fault currents and voltages compliant with the bushfire mitigation guidelines in [3]. The practical applications of the proposed NMPC is elaborated in the Supplementary Material.

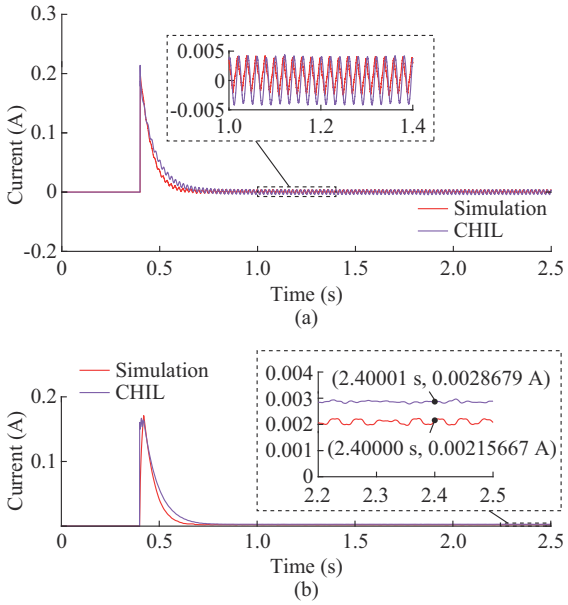

Fig. 21. Instantaneous and RMS values of fault current with $R_f = 26$ kΩ for CHIL validation. (a) Instantaneous values. (b) RMS values.

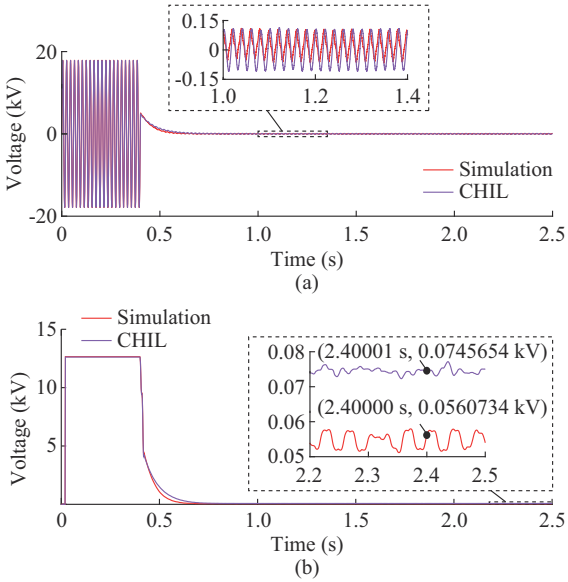

Fig. 22. Instantaneous and RMS values of faulty phase voltage with $R_f = 26$ kΩ for CHIL validation. (a) Instantaneous values. (b) RMS values.

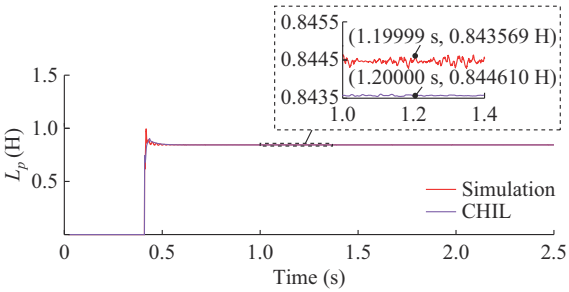

Fig. 23. Estimated value of L_p with $R_f = 26$ kΩ for CHIL validation.

VI. Conclusion

An NMPC is designed to compensate the SLG faults in RGPDNs. The proposed NMPC ensures the proper current injected into the neutral point by using the RCC inverter in an optimal way. The proposed NMPC has the following characteristics compared with other existing controllers.

1) The dynamic change in the adjustable inductor parameter is continuously monitored through the voltage and current measurements from the neutral points.

2) The fault compensation capability follows the timeframe as stated in the regulatory impact statement for the power line bushfire mitigation.

3) There is no requirement for a confined SS to ensure the robustness against parametric uncertainties.

The proposed NMPC utilizes the voltage and current measurements from the neutral point of the distribution network to estimate the value of the adjustable inductor, which is found to be slightly different from its nominal value and assists to improve the accuracy of injected current. This improved accuracy further helps compensate the faulty phase voltage and fault current. The rigorous analysis of results obtained from simulation and CHIL validations clearly highlights that the proposed NMPC is suitable to ensure the desired levels of fault compensation and it is practically applicable. Further research will also focus on automating the gain selection process using the AI based techniques.

References

[1] S. Tandon, S. Grijalva, and D. K. Molzahn, "Motivating the use of dynamic line ratings to mitigate the risk of wildfire ignition," in *Proceedings of 2021 IEEE Power and Energy Conference at Illinois* (*PECI*), Urbana, USA, Apr. 2021, pp. 1-7.

[2] D. Coldham, A. Czerwinski, and T. Marxsen, "Probability of bushfire ignition from electric arc faults," *Energy Safe Victoria*, Melbourne: Tech. Rep. HLC/2010/195, Dec. 2011.

[3] Acil Allen Consulting Pty Ltd. (2015, Nov.). Regulatory Impact Statement: bushfire mitigation regulations ammendment. [Online]. Available: https://acilallen.com.au/

[4] M. A. Barik, A. Gargoom, M. A. Mahmud *et al*., "A decentralized fault detection technique for detecting single phase to ground faults in power distribution systems with resonant grounding," *IEEE Transactions on Power Delivery*, vol. 33, no. 5, pp. 2462-2473, Oct. 2018.

[5] K. M. Winter, "The RCC ground fault neutralizer – a novel scheme for fast earth-fault protection," in *Proceedings of 18th International Conference and Exhibition on Electricity Distribution (CIRED 2005)*. Turin, Italy, Jun. 2005, pp. 1-4.

[6] M. Janssen, S. Kraemer, R. Schmidt *et al*., "Residual current compensation (RCC) for resonant grounded transmission systems using high performance voltage source inverter," in *Proceedings of 2003 IEEE PES Transmission and Distribution Conference and Exposition*, Dallas, USA, Sept. 2003, pp. 574-578.

[7] M. A. Barik, A. Gargoom, M. A. Mahmud *et al*., "Automatic network capacitive balancing technique for resonant grounded power distribution systems," *IET Generation*, *Transmission & Distribution*, vol. 14, no. 25, pp. 6158-6167, Dec. 2020.

[8] A. Gargoom, A. M. T. Oo, and M. Cavanagh, "A method for calculating the asymmetry in the shunt parameters of power lines in compensated distribution networks," *IEEE Transactions on Power Delivery*, vol. 35, no. 5, pp. 2168-2176, Oct. 2020.

[9] A. Cerretti, F. M. Gatta, A. Geri *et al*., "Ground fault temporary overvoltages in MV networks: evaluation and experimental tests," *IEEE Transactions on Power Delivery*, vol. 27, no. 3, pp. 1592-1600, Jul. 2012.

[10] H. Zeng, P. Yang, H. Cheng *et al*., "Research on single-phase to ground fault simulation base on a new type neutral point flexible grounding mode," *IEEE Access*, vol. 7, pp. 82563-82570, Jun. 2019.

[11] B. Fan, G. Yao, K. Yu *et al*., "Principle of flexible ground-fault arc suppression device based on zero-sequence voltage regulation," *IEEE Access*, vol. 9, pp. 2382-2389, Dec. 2020.

[12] M. Qi, H. Leng, Z. Zhang *et al*., "Fast disposal method for reducing electricity risk of single-phase ground fault in distribution network," in *Proceedings of 2017 China International Electrical and Energy Conference (CIEEC)*, Beijing, China, Oct. 2017, pp. 554-558.

[13] F. Wang, M. Guo, and G. Yang, "Novel arc-suppression methods based on cascaded H-bridge converter," in *Proceedings of 2016 Asia-Pacific International Symposium on Electromagnetic Compatibility (APEMC)*, Shenzhen, China, May 2016, pp. 691-694.

[14] A. Gargoom, M. A. Barik, M. A. Mahmud *et al*., "Residual current compensator based on voltage source converter for compensated distribution networks," in *Proceedings of 2018 IEEE PES General Meeting*, Portland, USA, Aug. 2018, pp. 1-5.

[15] Z. Y. Zheng, M. F. Guo, N. C. Yang *et al*., "Flexible arc-suppression method based on improved distributed commutations modulation for distribution networks," *International Journal of Electrical Power & Energy Systems*, vol. 116, p. 105580, Mar. 2020.

[16] W. Wang, L. Yan, X. Zeng *et al*., "Principle and design of a single-phase inverter-based grounding system for neutral-to-ground voltage compensation in distribution networks," *IEEE Transactions on Industrial Electronics*, vol. 64, no. 2, pp. 1204-1213, Feb. 2017.

[17] W. Wang, L. Yan, B. Fan *et al*., "Control method of an arc suppression device based on single-phase inverter," in *Proceedings of 2016 International Symposium on Power Electronics*, *Electrical Drives*, *Automation and Motion*, Anacapri, Italy, Jun. 2016, pp. 929-934.

[18] W. Wang, X. Zeng, L. Yan *et al*., "Principle and control design of active ground-fault arc suppression device for full compensation of ground current," *IEEE Transactions on Industrial Electronics*, vol. 64, no. 6, pp. 4561-4570, Jun. 2017.

[19] P. Wang, B. Chen, C. Tian *et al*., "A novel neutral electromagnetic hybrid flexible grounding method in distribution networks," *IEEE Transactions on Power Delivery*, vol. 32, no. 3, pp. 1350-1358, Jun. 2017.

[20] D. Chen, X. Zeng, S. Peng *et al*., "Active inverter device with double closed loop control method for arc suppression in distribution network," in *Proceedings of 2017 China International Electrical and Energy Conference*, Beijing, China, Oct. 2017, pp. 549-553.

[21] Y. Qu, W. Tan, and Y. Yang, "H-infinity control theory apply to new type arc-suppression coil system," in *Proceedings of 2007 7th International Conference on Power Electronics and Drive Systems*, Bangkok, Thailand, Nov. 2007, pp. 1753-1757.

[22] W. Q. Qiu, M. F. Guo, G. J. Yang *et al*., "Model-predictive-control-based flexible arc-suppression method for earth fault in distribution networks," *IEEE Access*, vol. 7, pp. 16051-16065, Jan. 2019.

[23] M. Barzegar-Kalashani and M. A. Mahmud, "A linear hybrid active disturbance rejection controller design to extenuate powerline bushfires in resonant grounded distribution power systems," *International Journal of Electrical Power & Energy Systems*, vol. 142, p. 108192, Nov. 2022.

[24] Z. Zheng, M. Guo, N. Yang *et al*., "FASD based on BSC method for distribution networks," *IET Generation*, *Transmission & Distribution*, vol. 13, no. 24, pp. 5487-5494, Dec. 2019.

[25] Z. Zheng, M. Guo, N. Yang *et al*., "Single-phase flexible arc suppression device based on BSC-SOGI-PLL method for distribution networks," *International Journal of Electrical Power & Energy Systems*, vol. 121, p. 106100, Oct. 2020.

[26] T. K. Roy, M. A. Mahmud, M. A. Barik *et al*., "A nonlinear backstepping control scheme for rapid earth fault current limiters in resonant grounded power distribution systems: applications for mitigating powerline bushfires," *IEEE Journal of Emerging and Selected Topics in Industrial Electronics*, vol. 3, no. 2, pp. 362-371, Apr. 2022.

[27] T. K. Roy, M. A. Mahmud, and N. K. Roy, "An integral backstepping controller design for compensated distribution networks with rapid earth fault current limiters in bushfire prone areas," *IET Generation*, *Transmission & Distribution*, vol. 16, no. 19, pp. 3928-3940, Oct. 2022.

[28] M. Barzegar-Kalashani, M. A. Mahmud, M. A. Barik *et al*., "Control of arc suppression devices in compensated power distribution systems using an integral sliding mode controller for mitigating powerline bushfires," *International Journal of Electrical Power & Energy Systems*, vol. 134, p. 107481, Nov. 2022.

[29] T. K. Roy, M. A. Mahmud, S. K. Ghosh *et al*., "Design of an adaptive sliding mode controller for rapid earth fault current limiters in resonant grounded distribution networks to mitigate powerline bushfires," in *Proceedings of 2021 IEEE Texas Power and Energy Conference*, College Station, USA, Feb. 2021, pp. 1-6.

[30] T. K. Roy and M. A. Mahmud, "Fault current compensations in reso-

nant grounded distribution systems to mitigate powerline bushfires using a nonsingular terminal sliding model controller," *IET Generation*, *Transmission & Distribution*, vol. 16, no. 3, pp. 479-491, Feb. 2022.
[31] T. K. Roy, M. A. Mahmud, A. B. M. Nasiruzzaman *et al*., "A non-singular fast terminal sliding mode control scheme for residual current compensation inverters in compensated distribution networks to mitigate powerline bushfires," *IET Generation*, *Transmission & Distribution*, vol. 15, no. 9, pp. 1421-1434, May 2021.
[32] T. K. Roy, M. A. Mahmud, A. B. M. Nasiruzzaman *et al*., "A hybrid sliding mode control scheme for rapid earth fault current limiters in compensated distribution networks in bushfire prone areas," *The Journal of Engineering*, vol. 2023, no. 3, pp. 1-12, Mar. 2023.
[33] T. K. Roy and M. A. Mahmud, "Control of arc suppression devices for reducing powerline bushfires in resonant grounded power distribution networks using global terminal sliding mode controller," *IET Generation*, *Transmission & Distribution*, vol. 17, no. 12, pp. 2773-2787, Jun. 2023.
[34] M. Barzegar-Kalashani, M. A. Mahmud, M. A. Barik *et al*., "A discrete sliding mode control scheme for arc suppression devices in resonant grounded power distribution systems to mitigate powerline bushfires," *Electric Power Systems Research*, vol. 210, p. 108126, Sept. 2022.
[35] W. S. P. Fernando, M. A. Mahmud, S. N. Islam *et al*., "A nonlinear model predictive controller design for residual current compensation inverters in rapid earth fault current limiters to mitigate powerline bushfires," *International Journal of Electrical Power & Energy Systems*, vol. 142, p. 108326, Nov. 2022.
[36] Y. Zhang, X. Liu, and B. Qu, "Distributed model predictive load frequency control of multi-area power system with DFIGs," *IEEE/CAA Journal of Automatica Sinica*, vol. 4, no. 1, pp. 125-135, Jan. 2017.
[37] M. S. Mahmoud and M. O. Oyedeji, "Adaptive and predictive control strategies for wind turbine systems: a survey," *IEEE/CAA Journal of Automatica Sinica*, vol. 6, no. 2, pp. 364-378, Mar. 2019.
[38] M. Kang, C. Wen, and C. Wu, "A model predictive scheduling algorithm in real-time control systems," *IEEE/CAA Journal of Automatica Sinica*, vol. 5, no. 2, pp. 471-478, Mar. 2018.
[39] M. Barzegar-Kalashani, B. Tousi, M. A. Mahmud *et al*., "Non-linear integral higher-order sliding mode controller design for islanded operations of T-type three-phase inverter-interfaced distributed energy resources," *IET Generation*, *Transmission & Distribution*, vol. 14, no. 1, pp. 53-61, Jan. 2020.
[40] L. Grne and J. Pannek, *Nonlinear Model Predictive Control: Theory and Algorithms*. Berlin: Springer, 2011.
[41] S. Devi and R. Seyezhai, "Simulation and analysis of modulation strategies for PV based T-type inverter," *International Journal of Pure and Applied Mathematics*, vol. 118, no. 24, pp. 1-18, Jun. 2018.

Warnakulasuriya Sonal Prashenajith Fernando received the Bachelor degree in electrical power engineering from Curtin University, Perth, Australia, in 2018. In 2021, he started pursuing the Ph.D. degree at Deakin University, Waurn Ponds, Australia, and he then moved to Northumbria University, Newcastle, UK, due to the relocation of his Ph. D. supervisor, where he is currently continuing his Ph.D. degree. His research interests include the resonant grounding techniques for power distribution networks, rapid earth fault current limiter, model-predictive control, adaptive-control, and extended state observer-based control.

Mostafa Barzegar-Kalashani received the B. Sc. degree in electrical engineering from Urmia University, Urmia, Iran, in 2012. He worked with Deakin University, Waurn Ponds, Australia, as a Research Assistant and currently, he is working at Swinburne University of Technolgy, Melbourne, Australia. His research interests include the nonlinear sliding model control theory and its applications to energy systems, wind energy conversion system, control of resonant grounded power distribution networks, and grid integration of renewable energy sources.

Md Apel Mahmud received the Bachelor degree in electrical engineering from Rajshahi University of Engineering & Technology, Rajshahi, Bangladesh, in 2008, with the University Gold Medal, and the Ph. D. degree in electrical engineering from the University of New South Wales, Sydney, Australia, in 2012, with the best thesis award. Currently, he is working as an Associate Professor in electrical engineering at Northumbria University, Newcastle, UK. Prior to joining Northumbria University, he worked as a Senior Lecturer and Lecturer in electrical & renewable energy engineering at Deakin University, Waurn Ponds, Australia. His research interests include dynamic stability and control of power systems, nonlinear control theory and applications, grid integration of renewable energy sources, and transactive energy management system.

Shama Naz Islam received the Ph. D. degree in engineering from the Australian National University (ANU), Canberra, Australia, in 2015. From 2010 to 2011, she had been a Lecturer in the Department of Electrical and Electronic Engineering in Bangladesh University of Engineering and Technology, Dhaka, Bangladesh. In March 2016, she joined the School of Engineering at Deakin University, Waurn Ponds, Australia, as a Lecturer. Her research interests include smart grid communication, wireless communication system, and peer-to-peer energy trading.

Nasser Hossenzadeh received the B. Sc. degree in electrical engineering from Shiraz University, Shiraz, Iran, in 1986, the M. Sc. degree in electronics engineering from the University of Science and Technology, Tehran, Iran, in 1992, and the Ph. D. degree in electrical power systems from Victoria University, Melbourne, Australia, in 1998. He is currently with Deakin University, Waurn Ponds, Australia, where he is leading the Centre for Smart Power and Energy Research (CSPER), School of Engineering. His research interests include stability assessment of the power grid as impacted by inverter-based resources (IBRs), microgrid, power system dynamics and control, online monitoring, real-time control of microgrids, and engineering education.